

1 **Perceived and mentally rotated contents are differentially represented**
2 **in cortical depth of V1**

3
4 Polina Iamshchinina^{a,b*}, Daniel Kaiser^c, Renat Yakupov^d, Daniel Haeneltⁱ, Alessandro Sciarra^{e,h}, Hendrik
5 Mattern^e, Falk Lüsebrink^{e,h}, Emrah Duezel^{d,g}, Oliver Speck^{d,e,f,g}, Nikolaus Weiskopf^{ij}, Radoslaw Martin
6 Cichy^{a,b}

7 ^a Department of Education and Psychology, Freie Universität Berlin, Habelschwerdter Allee 45, Berlin 14195,
8 Germany

9 ^b Berlin School of Mind and Brain, Humboldt-Universität zu Berlin, Unter den Linden 6, Berlin 10099, Germany

10 ^c Department of Psychology, University of York, Heslington, York, YO10 5DD, UK

11 ^d German Center for Neurodegenerative Diseases (DZNE), Leipziger Straße 44, Haus 64, Magdeburg 39120,
12 Germany

13 ^e Department of Biomedical Magnetic Resonance, Institute for Physics, Otto-von-Guericke-University,
14 Universitätsplatz 2, Magdeburg 39106, Germany

15 ^f Leibniz Institute for Neurobiology, Brennekestraße 6, Magdeburg 39118, Germany

16 ^g Center for Behavioral Brain Sciences, Universitätsplatz 2, G24-205, Magdeburg D-39106, Germany

17 ^h Department of Neurology, Otto-von-Guericke University, Leipziger Str. 44, Magdeburg 39120, Germany

18 ⁱ Department of Neurophysics, Max Planck Institute for Human Cognitive and Brain Sciences, Stephanstraße 1a,
19 Leipzig 04103, Germany

20 ^j Felix Bloch Institute for Solid State Physics, Faculty of Physics and Earth Sciences, Leipzig University, Linnéstraße
21 5, 04103 Leipzig, Germany

22

23 **Abstract**

24 Primary visual cortex (V1) in humans is known to represent both veridically
25 perceived external input and internally-generated contents underlying imagery and
26 mental rotation. However, it is unknown how the brain keeps these contents separate
27 thus avoiding a mixture of the perceived and the imagined which could lead to
28 potentially detrimental consequences. Inspired by neuroanatomical studies showing that
29 feedforward and feedback connections in V1 terminate in different cortical layers, we
30 hypothesized that this anatomical compartmentalization underlies functional segregation
31 of external and internally-generated visual contents, respectively. We used high-
32 resolution layer-specific fMRI to test this hypothesis in a mental rotation task. We found
33 that rotated contents were predominant at outer cortical depth bins (i.e. superficial and
34 deep). At the same time perceived contents were represented stronger at the middle
35 cortical bin. These results identify how through cortical depth compartmentalization V1
36 functionally segregates rather than confuses external from internally-generated visual
37 contents. These results indicate that feedforward and feedback manifest in distinct
38 subdivisions of the early visual cortex, thereby reflecting a general strategy for
39 implementing multiple cognitive functions within a single brain region.

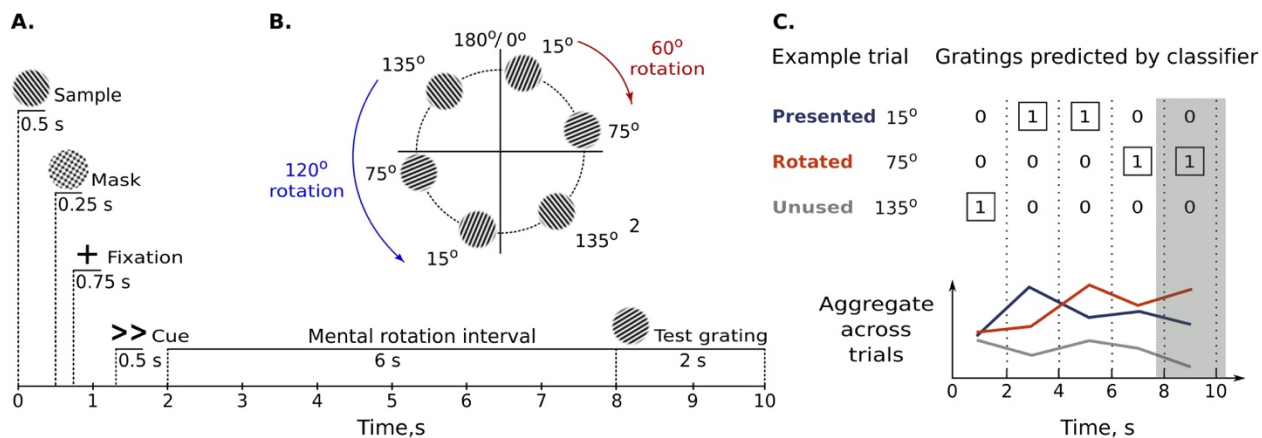
40 Introduction

41 Mental rotation is at the core of efficiently acting upon objects regardless of their
 42 orientation, such as when searching for a nail in a toolbox or solving a Rubik's cube. It
 43 comprises the perception of an external input and the internal generation of a
 44 transformed representation¹⁻³. Recent studies demonstrated that both operations are
 45 concurrently mediated by primary visual cortex⁴⁻⁵ (V1). Given this spatial overlap, how
 46 does the brain separate perception and mental rotation? Why do we not confuse
 47 perceived and mentally transformed contents?

48 Recent neuroanatomical studies suggest that projections carrying external and
 49 internally-generated signals in V1 are segregated across cortical layers. Feedforward
 50 projections terminate in the middle layer, while feedback connections terminate in
 51 superficial and deep layers⁶⁻¹¹. Studies of working memory and attention demonstrated
 52 the functional relevance of this layer-specific separation¹²⁻¹⁹. However, these studies
 53 measured the retention or amplification of the very stimuli previously represented in V1
 54 or estimated perception signal not concurrently but in a separate task. It is thus unclear
 55 how V1 separates presented from internally modified contents, such as during mental
 56 rotation.

57 Here, using high-resolution fMRI at 7T we show that the concurrent
 58 representation of perceived and mentally transformed contents during mental rotation is
 59 enabled by cortical depth separation of information in V1. The perceived contents were
 60 strongest at the middle cortical depth bins, while mentally rotated contents dominated in
 61 the superficial and deep cortical bins. These results show how the cognitive process of
 62 mental rotation is mediated by functionally distinct neural representations, explain why
 63 externally-induced and internally-generated contents are not confused, and supports the
 64 view of V1 as a dynamic 'blackboard' updated through connections from higher-order
 65 areas rather than a low-level stage of hierarchical processing.

66 Results



67

68 **Figure 1. Experimental methods. A.** On each trial, participants viewed a sample grating and then had 6
69 seconds to rotate it 60° (<, >) or 120° (<<, >>) to the left or to the right. After the mental rotation interval,
70 participants had 2 seconds to report whether a probe grating was tilted clockwise or counterclockwise
71 compared to the mentally rotated grating. **B.** We used a set of three stimuli, 15°, 75° and 135° oriented
72 gratings. As a result of the mental rotation, each stimulus could be turned into one of the other two stimuli.
73 For example, rotation of a 15° grating (red arrow) for 60° clockwise results in a 75° grating or rotation of a
74 135° grating (blue arrow) 120° counterclockwise results in a 15° grating. **C.** This panel shows classifiers'
75 decisions in an example trial, in which a 15° grating was rotated into a 75° grating. We aggregated results
76 across trials by counting how often classifiers predicted the presented orientation, the rotated orientation,
77 and the unused orientation. The shaded area denotes the time interval chosen for the in-depth analysis
78 (measurements at 8 and 10 seconds).

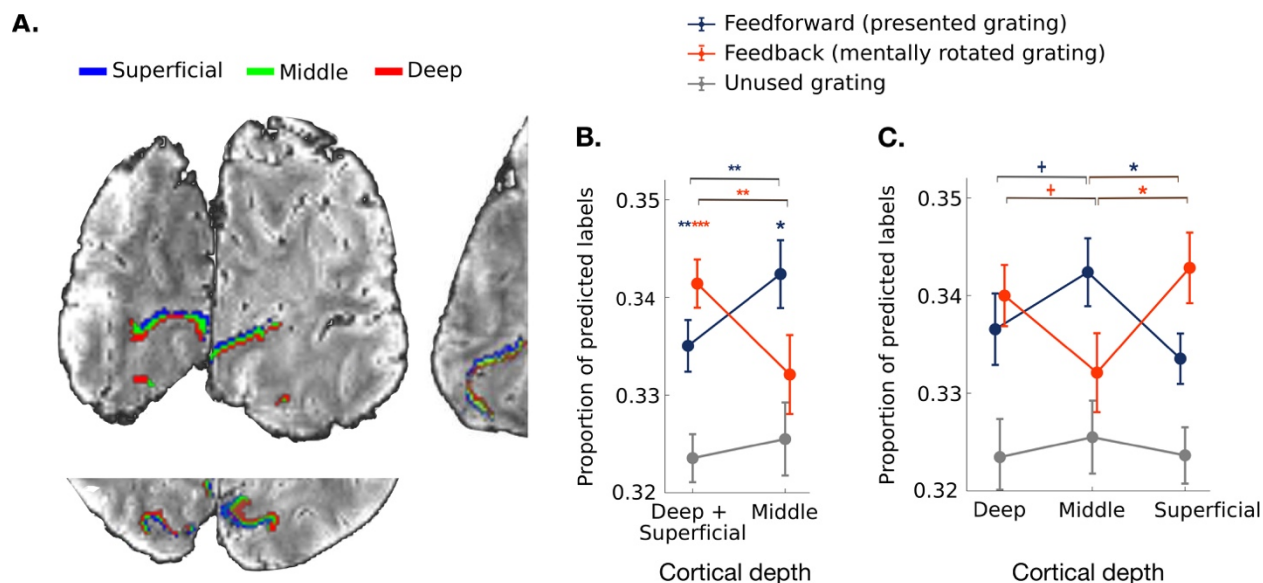
79 We recorded 7T fMRI with 0.8 mm iso voxel resolution while participants (n=23)
80 viewed and mentally rotated oriented gratings⁴. On each trial, we presented a single
81 grating (15°, 75°, or 135°), followed by a cue that instructed participants to mentally
82 rotate the presented grating to the left or to the right for either 60° or 120° (Figure 1A).
83 Thus, each of the orientations presented in the trial could be turned into one of the two
84 other orientations (Figure 1B). The presented and rotated gratings were different from
85 each other on every trial, allowing us to independently assess encoding of perceived
86 and mentally rotated contents. At the end of each trial, participants compared their
87 mental rotation result to probe grating with similar orientation. Behavioral data confirmed
88 that the participants could successfully perform this task, with greater reaction times
89 ($t_{23}=3.4$, $p=0.0012$) and error rates ($z=-1.64$, $p=0.06$) for the larger rotation angle¹.
90 (Supplementary Fig. 1A).

91 To examine depth-specific responses during mental rotation and perception, we
92 extracted three gray matter depth bins approximating deep, middle and superficial
93 cortical layers in V1 in every participant (Figure 2A, see Methods for further
94 clarification). For each depth bin, we trained support vector machine classifiers to
95 differentiate multi-voxel response patterns evoked by the three grating orientations.
96 Classifiers were always trained on response patterns in a separate block-design
97 localizer, during which participants saw the three orientations while performing an
98 orthogonal task (see Methods). These response patterns served as a benchmark for a
99 strong orientation-selective response in V1. Classifiers were then tested on response
100 patterns in the mental rotation experiment. To investigate representations of perceived
101 and rotated contents across time, we performed separate classification analyses for
102 every time point from stimulus onset to the end of the trial (5 TRs in total). We then
103 analysed the predicted orientation (15°, 75° or 135°) at each time point (Figure 1C). To
104 estimate the representational strength of the presented and rotated grating orientations,
105 we counted how often classifiers predicted (1) the presented orientation (e.g., predicting
106 15° on a trial where a 15° grating was rotated into a 75° grating), (2) the rotated
107 orientation (e.g., predicting 75° on a trial where a 15° grating was rotated into a 75°
108 grating), and (3) the third, unused orientation (e.g., predicting 135° on a trial where a
109 15° grating was rotated into a 75° grating). Accumulating the classifier predictions

110 across trials, we were able to track representations of perceived and mentally rotated
111 contents across cortical depths (see Methods).

112 We performed in-depth analyses in the time interval from 8 to 10 seconds (i.e., 2
113 TRs) after the rotation cue. This time interval was pre-selected based on previous
114 studies⁴⁻⁵ where the mentally rotated gratings could be decoded starting from 8 seconds
115 following the rotation instruction (also see Methods for further clarification). Previous
116 fMRI studies^{14,20,38} however utilized different time intervals and experimental tasks to
117 show the distribution of feedforward and feedback signals in cortical depth (for the
118 perception signal decoding based on orientation localizer task in our study see
119 Supplementary Fig. 2). Building on this previous work, our main goal here was to
120 disentangle concurrent representations of perceived and mentally rotated contents
121 across cortical depth, even when they are represented in a spatially and temporally
122 overlapping way.

123



124

125 **Figure 2. Results.** **A.** Coronal, axial and sagittal slices of the average EPI image of a representative
126 participant, overlaid with cortical depth bins approximating cortical layers (superficial, middle and deep)
127 from an equi-volume model (see Methods). The cortex is mapped within the region of V1 with voxel
128 eccentricity values 0-3°. **B.** Classifier decisions in V1 over the time interval measured at 8 and 10
129 seconds after the rotation onset for the presented, mentally rotated and unused gratings in the outer
130 cortical bins (average of the superficial and deep bin) and the middle cortical bin (see Supplementary Fig.
131 3 for detailed analysis within an extended time interval and Supplementary Fig. 4 for analyses across all
132 time points). Perceptual contents were more strongly represented at the middle cortical depth, whereas
133 mentally rotated contents were dominant at the outer cortical bin. **C.** Comparing classifier decisions
134 between all three cortical bins (superficial vs. middle vs. deep) reveals that the difference between
135 perceived and rotated contents is most pronounced between the middle and superficial depths. All error
136 bars denote standard error of mean over subjects. +: $p < 0.09$, *: $p < 0.05$, **: $p < 0.01$, ***: $p < 0.001$.

137 Firstly, we hypothesized that representations of mentally rotated and perceived contents
138 should emerge at the outer and middle cortical depth bins, respectively. To test this

139 hypothesis, we compared the mental rotation and perception signals to the unused
140 grating in the average of the outer bins and in the middle bin (Figure 2B, see Methods
141 for the clarification for the choice of the baseline). We found significantly more classifier
142 choices for the rotated grating in the outer cortical bins ($t_{22}=4.6$, $p=0.0001$, Cohen's $d =$
143 0.97 , FDR-corrected for the number of cortical bins), but not at the middle depth
144 ($t_{22}=0.2$, $p=0.9$). Classifier choices for the presented grating were significantly more
145 frequent than for the unused grating at the middle depth ($t_{22}=2.8$, $p= 0.014$, Cohen's d
146 $= 0.59$) as well as in the outer depth bins ($t_{22}=2.7$, $p= 0.006$, Cohen's $d = 0.56$). In sum,
147 mentally rotated contents reached significance only in the outer cortical bins, whereas
148 perception signal was present at all the cortical bins.

149 To compare mental rotation and perception signals across cortical depth bins, we
150 ran a repeated-measures ANOVA with factors Signal Type (perception vs. mental
151 rotation) and Cortical Depth (middle vs. outer cortical bins) (Figure 2B). The analysis
152 revealed a significant interaction ($F_{1,22}=10.95$, $p=0.0045$). More information about the
153 rotated orientation was found in the outer cortical bins than at the middle depth
154 ($t_{22}=2.52$, $p=0.0096$, Cohen's $d=0.53$). In contrast, more information about the perceived
155 orientation was present at the middle bin than in the outer bins ($t_{22}=2.8$, $p=0.0052$,
156 Cohen's $d=0.58$). Similar distribution of feedforward signal was observed in V2
157 (Supplementary Fig. 5). We conclude that information about perceived and mentally
158 rotated contents in V1 is spatially separated across cortical depth bins and functionally
159 corresponds to cortical layers: the outer bins in our study mainly represented mentally
160 generated contents and the middle bin selectively encoded sensory information.

161 As superficial and deep cortical depth bins were aggregated in the
162 aforementioned analyses, we performed an additional analysis comparing all three
163 depth compartments (deep vs. middle vs. superficial). A repeated-measures ANOVA
164 again revealed a significant interaction between Signal Type and Cortical Depth
165 ($F_{2,44}=5.3$, $p=0.0085$) (Figure 2C). Unpacking this, mentally rotated orientation was more
166 strongly represented in the superficial cortical bin than in the middle one ($t_{22}=2.7$,
167 $p=0.02$, Cohen's $d=0.56$) and more strongly in the deep bin than at the middle cortical
168 depth (again at the trend level; $t_{22}=2.7$, $p=0.08$, Cohen's $d=0.35$). In contrast, the
169 perceived orientation was more strongly represented in the middle bin than at the
170 superficial ($t_{22}=2.9$, $p=0.014$, Cohen's $d=0.6$) and deep ones (at the trend level; $t_{22}=1.8$,
171 $p=0.06$, Cohen's $d=0.38$). No statistically significant difference between the deep and
172 superficial depth bins was found when analyzing representations of perceived ($t_{22}=0.86$,
173 $p=0.19$) or mentally rotated gratings ($t_{22}=0.6$, $p=0.27$). Mentally rotated contents were
174 thus represented in both outer depth bins, albeit weaker dissociations emerged between
175 the middle and the deep cortical bins.

176 Discussion

177 Harnessing the fine-grained resolution of 7T fMRI, we were able to resolve the
178 functional segregation of signals underlying mentally rotated and perceived contents in
179 V1: perceptual signals were dominant at the middle depth of V1, whereas mentally
180 rotated contents were found in the superficial and deep bins. While our results are
181 consistent with the previous fMRI studies at the standard resolution showing that V1
182 houses representations of both perceived and mentally rotated contents⁴⁻⁵
183 (Supplementary Fig. 1B), our findings provide the first functional explanation for
184 externally-induced and internally-generated representations during mental rotation
185 overlapping on a 2D map of cortex, yet functionally distinct in a 3D cortical model.

186 The functional separation of the contents of perception and mental rotation into
187 cortical depth bins follows the neuroanatomy of V1, which is characterized by bottom-up
188 connections terminating in the middle cortical layer and top-down connections
189 terminating in the outer layers⁶⁻¹¹. Our results demonstrate that this anatomical
190 differentiation between feedforward and feedback connections directly maps onto
191 activity time courses during a cognitive task. A similar mapping between fine-scale
192 cortical architecture and bottom-up and top-down information flow underpins basic
193 visual functions such as illusory perception²⁰⁻²¹ and visual expectations²². Although
194 different involvements of superficial and deep cortical depths were reported in these
195 studies, they consistently highlight a laminar separation between the middle and the
196 outer cortical subdivisions in V1. Specifically, a more pronounced representation of the
197 feedback signal at the superficial cortical depth in our study could potentially result from
198 different underlying processes. First of all, this finding is consistent with the previous
199 studies^{20,21,38} where feedback signal was measured in the presence of physical stimuli.
200 In our experiment, perceptual stimuli were only briefly shown at the trial onset, but
201 perception contents were reliably represented in the brain activity patterns throughout
202 the trial duration and thereby could impact the depth distribution of the feedback signal.
203 Another possibility is that fMRI measurements obtained with gradient-echo sequence in
204 our study could be biased towards superficial cortical depth due to close proximity to
205 pial veins (effect of draining veins)^{40,42,43} resulting in comparatively stronger
206 dissociations between the middle and superficial cortical bins.

207 We demonstrated that perception contents are more strongly represented at the
208 middle depth when estimated concurrently with mentally rotated contents, while no such
209 difference was observed in the absence of feedback manipulation (Supplementary Fig.
210 2). This result points to a separation of feedforward and feedback signals by cortical
211 depth in V1 possibly in order to avoid confusion between the two information streams. A
212 similar result was obtained in a recent study which concurrently manipulated feature-
213 based attention (top-down) and stimulus contrast (bottom-up)¹⁵, suggesting that the

214 observed functional signal-by-layer separation may be a general cortical mechanism
215 (also in primates³⁴).

216 The involvement of V1 in dynamically representing internally-generated contents
217 invites a redefinition of the region's role for visual cognition. Our results support the view
218 that V1 is not only a sophisticated feature processor for sensory input passing through,
219 but rather a high-resolution buffer that can be dynamically updated through connections
220 from higher-order areas. The view of V1 as a dynamic "blackboard"^{23,24} is consistent
221 with studies reporting V1 activations when stimulation is absent²⁵⁻²⁷, when participants
222 direct attention without visual inputs²⁸, and after stimulating other modalities²⁹, even in
223 the blind^{30,31}.

224 Although supporting the dynamic "blackboard" view, our results confront the idea
225 of a 'perception-like' nature of mental images^{24,32}, indicating that feedforward and
226 feedback mechanisms manifest in distinct neural populations of V1. This dissociation of
227 information flow by cortical depth questions the idea of 'shared representation' for
228 mental rotation and perception pointing towards a necessity for further clarification of
229 the properties that are common or instead uniquely owned by each process. For this,
230 future studies are needed to systematically compare perceived and mentally rotated
231 representations in the middle³³ and outer cortical layers, for example, through
232 contrasting perception- and imagery-induced retinotopic maps of low-level features such
233 as horizontal/vertical meridian, foveal/parafoveal cortical divisions, or orientation
234 discrimination biases.

235 Beyond the spatial separation of perceived and mentally rotated contents, the
236 laminar organization of feedforward and feedback information may also facilitate
237 interactions between these signals. Processing bottom-up and top-down signals in close
238 physical proximity on the cortical surface optimizes cross-talk that is essential for a large
239 set of cognitive functions such as figure-ground segregation^{16,34}, surround
240 suppression³⁵, visual attention¹⁷⁻¹⁹ and visual short-term memory^{12,14,36}. In fact,
241 predictive coding accounts suggest that a multitude of brain processes depend on such
242 interactions^{37,38,39}, rendering the laminar separation of feedforward and feedback
243 information a candidate for an implementation strategy for various other brain functions.

244 Layer-specific fMRI is an emerging technique requiring further procedure
245 stabilization and refinement of analysis to ensure that obtained results are not impacted
246 by motion artifacts (see Methods), draining veins effect or data acquisition methods
247 potentially introducing resolution losses⁴¹. We acknowledge a potential influence of
248 these factors on our results, and future studies using alternative protocols⁴⁴ to alleviate
249 potential confounds are required to accrue additional evidence.

250 Although our study highlights that V1 represents internally-generated contents, a
251 firm link between such V1 representations and the subjective quality of mental images is
252 yet to be established. Future studies could directly link fine-grained cortical feedback
253 patterns to an individual's ability to successfully conjure up mental representations

254 during mental rotation⁴⁵⁻⁴⁷ and mental imagery^{48,49}. Such studies may also help to
255 reveal imbalances between feedforward and feedback signals that lead to aphantasia⁵⁰⁻
256⁵², hallucinations or other perceptual disturbances^{53,54} - and eventually treat these
257 symptoms in the future.

258 Together, our results elucidate how the contents of perception and mental
259 rotation are simultaneously represented in different cortical compartments of V1. Our
260 findings thereby highlight that early visual cortex is not only involved in the analysis of
261 sensory inputs but is also recruited during dynamic visual cognition. Separating these
262 different functions across cortical depth may reflect a general strategy for implementing
263 multiple cognitive functions within a single brain region.

264 References

- 265 1. Shepard, R. N., & Metzler, J. (1971). Mental rotation of three-dimensional objects. *Science*,
266 171(3972), 701-703.
- 267 2. Cooper, L. A. (1975). Mental rotation of random two-dimensional shapes. *Cognitive psychology*, 7(1),
268 20-43.
- 269 3. Cooper, L. A., & Podgorny, P. (1976). Mental transformations and visual comparison processes:
270 Effects of complexity and similarity. *Journal of Experimental Psychology: Human Perception and*
271 *Performance*, 2(4), 503-514.
- 272 4. Albers, A. M., Kok, P., Toni, I., Dijkerman, H. C., & De Lange, F. P. (2013). Shared representations
273 for working memory and mental imagery in early visual cortex. *Current Biology*, 23(15), 1427-1431.
- 274 5. Christophel, T. B., Cichy, R. M., Hebart, M. N., & Haynes, J. D. (2015). Parietal and early visual
275 cortices encode working memory content across mental transformations. *Neuroimage*, 106, 198-206.
- 276 6. Rockland, K. S., & Pandya, D. N. (1979). Laminar origins and terminations of cortical connections of
277 the occipital lobe in the rhesus monkey. *Brain Research*, 179(1), 3-20.
- 278 7. Lund, J. S. (1988). Anatomical organization of macaque monkey striate visual cortex. *Annual review*
279 *of neuroscience*, 11(1), 253-288.
- 280 8. Van Essen, D. C., & Felleman, D. J. (1991). Distributed Hierarchical Processing in the Primate
281 Cerebral Cortex. *Cerebral Cortex*, 1, 1-47. Retrieved from
282 <http://www.cns.nyu.edu/~tony/vns/readings/felleman-vanessen-1991.pdf>
- 283 9. Markov, N. T., Ercsey-Ravasz, M., Van Essen, D. C., Knoblauch, K., Toroczkai, Z., & Kennedy, H.
284 (2013). Cortical high-density counterstream architectures. *Science*, 342(6158).
285 <https://doi.org/10.1126/science.1238406>
- 286 10. Markov, N. T., Vezoli, J., Chameau, P., Falchier, A., Quilodran, R., Huissoud, C., ... Kennedy, H.
287 (2014). Anatomy of hierarchy: Feedforward and feedback pathways in macaque visual cortex. *Journal*
288 *of Comparative Neurology*, 522(1), 225-259. <https://doi.org/10.1002/cne.23458>
- 289 11. Harris, K. D., & Mrsic-Flogel, T. D. (2013). Cortical connectivity and sensory coding. *Nature*,
290 503(7474), 51-58. <https://doi.org/10.1038/nature12654>
- 291 12. van Kerkoerle, T., Self, M. W., & Roelfsema, P. R. (2017). Layer-specificity in the effects of attention
292 and working memory on activity in primary visual cortex. *Nature Communications*, 8, 13804.
293 <https://doi.org/10.1038/ncomms13804>
- 294 13. van Kerkoerle, T., Self, M. W., & Roelfsema, P. R. (2014). Effects of attention and working memory in
295 the different layers of monkey primary visual cortex. *Soc.Neurosci.Abstr.*, 8, 263.13.
296 <https://doi.org/10.1038/ncomms13804>

- 297 14. Lawrence, S. J., van Mourik, T., Kok, P., Koopmans, P. J., Norris, D. G., & de Lange, F. P. (2018).
298 Laminar organization of working memory signals in human visual cortex. *Current Biology*, 28(21),
299 3435-3440.
- 300 15. Lawrence, S. J., Norris, D. G., & De Lange, F. P. (2019). Dissociable laminar profiles of concurrent
301 bottom-up and top-down modulation in the human visual cortex. *Elife*, 8, e44422.
- 302 16. Poort, J., Raudies, F., Wannig, A., Lamme, V. A., Neumann, H., & Roelfsema, P. R. (2012). The role
303 of attention in figure-ground segregation in areas V1 and V4 of the visual cortex. *Neuron*, 75(1), 143-
304 156.
- 305 17. Roelfsema, P. R., Lamme, V. A., & Spekreijse, H. (1998). Object-based attention in the primary visual
306 cortex of the macaque monkey. *Nature*, 395(6700), 376-381.
- 307 18. Klein, B. P., Fracasso, A., van Dijk, J. A., Paffen, C. L. E., te Pas, S. F., & Dumoulin, S. O. (2018).
308 Cortical depth dependent population receptive field attraction by spatial attention in human V1.
309 *NeuroImage*, 176(October 2017), 301–312. <https://doi.org/10.1016/j.neuroimage.2018.04.055>
- 310 19. Guo, F., Liu, C., Qian, C., Zhang, Z., Sun, K., Wang, D. J., ... & Zhang, P. Layer-dependent
311 multiplicative effects of spatial attention on contrast responses in human early visual cortex. Preprint
312 at: <https://www.biorxiv.org/content/biorxiv/early/2020/02/02/2020.02.01.926303.full.pdf> (2020).
- 313 20. Kok, P., Bains, L. J., Van Mourik, T., Norris, D. G., & De Lange, F. P. (2016). Selective activation of
314 the deep layers of the human primary visual cortex by top-down feedback. *Current Biology*, 26(3),
315 371–376. <https://doi.org/10.1016/j.cub.2015.12.038>
- 316 21. Bergmann, J., Morgan, A. T., & Muckli, L. Two distinct feedback codes in V1 for ‘real’ and ‘imaginary’
317 internal experiences. Preprint at:
318 <https://www.biorxiv.org/content/biorxiv/early/2019/06/13/664870.full.pdf>, 664870 (2019).
- 319 22. Aitken, F., Menelaou, G., Warrington, O., Koolschijn, R. S., Corbin, N., Callaghan, M. F., & Kok, P.
320 Prior expectations evoke stimulus templates in the deep layers of V1. Preprint at:
321 <https://www.biorxiv.org/content/10.1101/2020.02.13.947622v1.full.pdf> (2020).
- 322 23. Bullier J. 2001. Integrated model of visual processing. *Brain Res. Brain Res. Rev.* 36:96–107
- 323 24. Roelfsema, P. R., & de Lange, F. P. (2016). Early visual cortex as a multiscale cognitive blackboard.
324 *Annual review of vision science*, 2, 131-151.
- 325 25. Smith, F. W., & Muckli, L. (2010). Nonstimulated early visual areas carry information about
326 surrounding context. *Proceedings of the National Academy of Sciences*, 107(46), 20099-20103.
- 327 26. Mechelli, A., Price, C. J., Friston, K. J., & Ishai, A. (2004). Where bottom-up meets top-down:
328 neuronal interactions during perception and imagery. *Cerebral cortex*, 14(11), 1256-1265.
- 329 27. Dijkstra, N., Zeidman, P., Ondobaka, S., van Gerven, M. A., & Friston, K. (2017). Distinct top-down
330 and bottom-up brain connectivity during visual perception and imagery. *Scientific reports*, 7(1), 1-9.
- 331 28. Kastner, S., Pinsk, M. A., De Weerd, P., Desimone, R., & Ungerleider, L. G. (1999). Increased activity
332 in human visual cortex during directed attention in the absence of visual stimulation. *Neuron*, 22(4),
333 751-761.
- 334 29. Vetter, P., Smith, F. W., & Muckli, L. (2014). Decoding sound and imagery content in early visual
335 cortex. *Current Biology*, 24(11), 1256-1262.
- 336 30. Amedi, A., Raz, N., Pianka, P., Malach, R., & Zohary, E. (2003). Early ‘visual’ cortex activation
337 correlates with superior verbal memory performance in the blind. *Nature neuroscience*, 6(7), 758-766.
- 338 31. Vetter, P., Bola, Ł., Reich, L., Bennett, M., Muckli, L., & Amedi, A. (2020). Decoding Natural Sounds
339 in Early “Visual” Cortex of Congenitally Blind Individuals. *Current Biology*.
- 340 32. Dijkstra, N., Bosch, S. E., & van Gerven, M. A. (2019). Shared neural mechanisms of visual
341 perception and imagery. *Trends in cognitive sciences*, 23(5), 423-434.
- 342 33. Polimeni, J. R., Fischl, B., Greve, D. N., & Wald, L. L. (2010). Laminar analysis of 7 T BOLD using an
343 imposed spatial activation pattern in human V1. *Neuroimage*, 52(4), 1334-1346.

- 344 34. Self, M. W., van Kerkoerle, T., Supèr, H., & Roelfsema, P. R. (2013). Distinct roles of the cortical
345 layers of area V1 in figure-ground segregation. *Current Biology*, 23(21), 2121-2129.
- 346 35. Bijanzadeh, M., Nurminen, L., Merlin, S., Clark, A. M., & Angelucci, A. (2018). Distinct laminar
347 processing of local and global context in primate primary visual cortex. *Neuron*, 100(1), 259-274.
- 348 36. Rademaker, R. L., Chunharas, C., & Serences, J. T. (2019). Coexisting representations of sensory
349 and mnemonic information in human visual cortex. *Nature neuroscience*, 22(8), 1336-1344. Hgfv
- 350 37. Bastos, A. M., Usrey, W. M., Adams, R. A., Mangun, G. R., Fries, P., & Friston, K. J. (2012).
351 Canonical microcircuits for predictive coding. *Neuron*, 76(4), 695-711.
- 352 38. Muckli, L., De Martino, F., Vizioli, L., Petro, L. S., Smith, F. W., Ugurbil, K., ... Yacoub, E. (2015).
353 Contextual Feedback to Superficial Layers of V1. *Current Biology*, 25(20), 2690-2695.
354 <https://doi.org/10.1016/j.cub.2015.08.057>
- 355 39. Stephan, K. E., Petzschner, F. H., Kasper, L., Bayer, J., Wellstein, K. V., Stefanics, G., ... & Heinzle,
356 J. (2019). Laminar fMRI and computational theories of brain function. *Neuroimage*, 197, 699-706.
- 357 40. Self, M. W., van Kerkoerle, T., Goebel, R., & Roelfsema, P. R. (2019). Benchmarking laminar fMRI:
358 neuronal spiking and synaptic activity during top-down and bottom-up processing in the different
359 layers of cortex. *Neuroimage*, 197, 806-817.
- 360 41. Bause, J., Polimeni, J. R., Stelzer, J., In, M. H., Ehse, P., Kraemer-Fernandez, P., ... & Scheffler, K.
361 (2020). Impact of prospective motion correction, distortion correction methods and large vein bias on
362 the spatial accuracy of cortical laminar fMRI at 9.4 Tesla. *Neuroimage*, 208, 116434.
- 363 42. Heinzle, J., Koopmans, P. J., den Ouden, H. E., Raman, S., & Stephan, K. E. (2016). A hemodynamic
364 model for layered BOLD signals. *Neuroimage*, 125, 556-570.
- 365 43. Uludağ, K., & Blinder, P. (2018). Linking brain vascular physiology to hemodynamic response in ultra-
366 high field MRI. *Neuroimage*, 168, 279-295.
- 367 44. Chai, Y., Li, L., Huber, L., Poser, B. A., & Bandettini, P. A. (2020). Integrated VASO and perfusion
368 contrast: A new tool for laminar functional MRI. *Neuroimage*, 207, 116358.
- 369 45. Just, M. A., & Carpenter, P. A. (1985). Cognitive coordinate systems: accounts of mental rotation and
370 individual differences in spatial ability. *Psychological review*, 92(2), 137.
- 371 46. Roberts, J. E., & Bell, M. A. (2000). Sex differences on a mental rotation task: variations in
372 electroencephalogram hemispheric activation between children and college students. *Developmental*
373 *neuropsychology*, 17(2), 199-223.
- 374 47. Khooshabeh, P., Hegarty, M., & Shipley, T. F. (2013). Individual differences in mental rotation:
375 Piecemeal versus holistic processing. *Experimental psychology*, 60(3), 164.
- 376 48. Pearson, J. (2019). The human imagination: the cognitive neuroscience of visual mental imagery.
377 *Nature Reviews Neuroscience*, 20(10), 624-634.
- 378 49. Fulford, J., Milton, F., Salas, D., Smith, A., Simler, A., Winlove, C., & Zeman, A. (2018). The neural
379 correlates of visual imagery vividness—An fMRI study and literature review. *Cortex*, 105, 26-40.
- 380 50. Zeman, A., Milton, F., Della Sala, S., Dewar, M., Frayling, T., Gaddum, J., ... & Winlove, C. (2020).
381 Phantasia—The Psychological Significance Of Lifelong Visual Imagery Vividness Extremes. *Cortex*.
- 382 51. Bainbridge, W. A., Pounder, Z., Eardley, A. F., & Baker, C. I. (2021). Quantifying Aphantasia through
383 drawing: Those without visual imagery show deficits in object but not spatial memory. *Cortex*, 135,
384 159-172.
- 385 52. Pounder, Z., Jacob, J., Jacobs, C., Loveday, C., Towell, T., & Silvanto, J. (2018). Mental rotation
386 performance in aphantasia. *Journal of Vision*, 18(10), 1123-1123.
- 387 53. Horga, G., Schatz, K. C., Abi-Dargham, A., & Peterson, B. S. (2014). Deficits in predictive coding
388 underlie hallucinations in schizophrenia. *Journal of Neuroscience*, 34(24), 8072-8082.
- 389 54. Haarsma, J., Kok, P., & Browning, M. (2020). The promise of layer-specific neuroimaging for testing
390 predictive coding theories of psychosis. Preprint at: <https://psyarxiv.com/5p64f/> (2020).

391 **Methods**

392 1.1. Participants

393 Twenty-five healthy adults (age Mean \pm SD: 29 \pm 5.7; 9 female) participated in the
394 study. All participants had normal or corrected-to-normal vision. Participants gave their
395 written informed consent for participation in the study as well as for publicly sharing all
396 obtained data in pseudonymized form. They received monetary reimbursement for their
397 participation. The study was approved by the ethics committee of the Otto-von-
398 Guericke-University Magdeburg, Germany. Two participants had to be excluded due to
399 aborted data collection and artifacts in the anatomical T1-weighted image, respectively.
400 All analyses were conducted on the remaining twenty-three participants.

401 We chose the number of subjects that was similar or exceeded the sample sizes
402 of previous 7T studies investigating feedback signals with laminar separation^{14,15,18,20,38}.

403 1.2. Stimuli

404 Stimuli were grayscale luminance-defined sinusoidal gratings generated using
405 MATLAB (MathWorks, Natick, MA) in conjunction with the Psychophysics Toolbox¹.
406 The gratings were presented in an annulus (outer diameter: 6.7° of visual angle, inner
407 diameter: 1.3° of visual angle) surrounding a central fixation point. The gratings had a
408 spatial frequency of 2 cpd (12.34 Hz) and a Michelson contrast of 100%. Stimuli were
409 displayed on an LCD projector (DLR-RS49E, JVC Ltd.) on a rear-projection screen
410 positioned behind the head coil within the magnet bore. Participants viewed the screen
411 through a mirror attached to the head coil.

412 1.3. Experimental procedure

413 1.3.1. Training procedure

414 Before entering the MRI scanner, participants underwent a training procedure
415 which comprised minimum 4 runs for all the participants, with 6 being the maximum
416 number in case participants needed more time to learn how to perform the task. At the
417 start of each trial, participants briefly saw a randomly oriented grating (Figure 1A). The
418 stimulus presentation was followed by a mask comprising the intersection of three
419 gratings (15°,75°,135°) at random phase. A subsequently presented task cue indicated
420 which direction participants had to rotate the presented stimulus grating in their mind's
421 eye. Mental rotation could go either clockwise or counterclockwise (as indicated by
422 arrow direction), and for 60 or 120° (as indicated by the number of arrows). After a 6
423 second rotation period a probe grating was shown. The probe comprised the grating
424 shown in the beginning of the trial, rotated in accordance with the cue instruction.
425 Additionally, the grating was slightly tilted clockwise or counterclockwise; the amount of
426 additional tilt was regulated using staircase procedure (described below). The

427 participants' task was to indicate the direction of difference between the probe grating
428 and the mentally rotated grating. After each trial, participants received a 1 second
429 feedback about their performance. The inter-trial interval was 2 seconds. Each training
430 run consisted of 36 trials and took 7 minutes 52 seconds. At the end of each run,
431 participants received feedback about their average accuracy.

432 1.3.2. Staircase Procedure

433 To maintain a sensitive accuracy range, the extent of additional tilt in the test
434 stimulus, (compared to the orientation resulting from the mental rotation) was adjusted
435 using a staircase procedure. The initial difference between the orientation resulting from
436 mental rotation and probe grating was set at 20°. For each correct response in a given
437 trial, the difference between the probe and rotated grating was reduced by 0.5°, making
438 orientation discrimination harder. Conversely, the difference was increased by 2° for
439 each incorrect response, making discrimination easier. We imposed an upper limit of
440 40° on the orientation difference. The staircase procedure continued across the whole
441 experiment, including the training runs and the fMRI experiment.

442 1.3.3. Experimental task

443 In the scanner, participants first underwent an anatomical scanning procedure,
444 during which we acquired two T1-weighted anatomical scans, two PD-weighted
445 contrasts and a T2-weighted contrast (described in more detail in 'Parameters of Data
446 Acquisition'). The anatomical scanning procedure took approximately 40 min. During
447 anatomical scan procedure participants were encouraged to rest and move as least as
448 possible to reduce motion artefacts.

449 After that, participants continued to perform the task, which they were trained in
450 beforehand (Figure 1A), but with two major changes. First, participants did not receive
451 feedback on their performance to increase the number of trials during scanning time.
452 Second, the sample gratings shown at the beginning of each trial were no longer
453 randomly oriented, but limited to 15°, 75° or 135° orientation from the vertical axis. We
454 limited the number of possible stimuli compared to the training session to increase
455 signal-to-noise ratio per each sample grating and to enable signal differentiation at the
456 level of cortical depth bins. In future studies, the use of richer stimulus sets may provide
457 insight to whether the same neural processes, which govern the mental rotation tasks,
458 are also performed on everyday objects during our daily lives.

459 We generated a cyclical design, that is, each of these orientations could be
460 turned into one of the two other orientations on a circle defined by stimulus orientation
461 (Figure 1B). In effect, the presented and rotated gratings were different from each other
462 on every trial, allowing us to independently assess encoding of perceived and mentally
463 rotated contents.

464 Overall, there were three possible starting orientations (15°, 75° or 135°), two
465 directions of rotation (clockwise or counter-clockwise) and two rotation magnitudes (60°
466 or 120°), resulting in 12 unique trial types. The 12 unique trials were repeated 3 times
467 within each run, resulting in a total of 36 trials. Trial order was fully randomized. In a
468 nutshell, the experiment consisted of 6 runs, which each lasted 7 minutes 16 seconds.

469 We cannot ultimately exclude the possibility that participants realized how many
470 stimuli were shown overall and only retrieved the relevant orientation from memory
471 rather than performing the rotation task properly. Such strategies are a typical problem
472 in mental rotation studies using a fixed number of repeating stimuli. However, our
473 behavioral data provides direct evidence against this scenario: the response time data
474 cannot be accounted for by the retrieval of fixed orientations (or orientation) labels from
475 memory. We would like to add that after the experiment, we asked each participant how
476 many orientations they had to rotate and none of them reported the real number of
477 orientations in the stimulus set. Therefore, we believe that our participants were
478 genuinely performing the mental rotation task.

479 1.3.4. Orientation localizer task

480 To select voxels most responsive to each of the three orientations shown in the
481 experiment, participants finally completed an additional orientation localizer run. During
482 this run, gratings with the three orientations (15°, 75° and 135°) were shown in a block
483 design in a pseudo-randomized order. In each block, one of the grating orientations was
484 shown for 12 seconds, flickering at 4 Hz. Every three blocks (i.e., one repeat of the
485 three orientations) were followed by a fixation block, which lasted 15 seconds.
486 Participants had to monitor the fixation cross for occasional brief changes in color, to
487 which they had to respond with a button press. Overall, we recorded data for 60 blocks
488 (45 orientation blocks and 15 fixation blocks). The fixation dot changed 9-10 times per
489 block at random time points, leading to approximately 144 changes, to which
490 participants responded on average 94+/-4% (Mean ± SD) of the time. The orientation
491 localizer task was performed last in the experiment to ensure that participants did not
492 notice that the orientations shown to them during prolonged periods in the localizer task
493 (12 s) are the same three orientations as the ones briefly presented in the beginning of
494 each trial of the main experiment. The localizer task took 12 minutes 49 seconds. The
495 average time for completing the whole experiment was 115 minutes including
496 anatomical scans.

497 1.4. Parameters of data acquisition

498 MRI data were acquired using a 7T Siemens whole-body MR scanner (7T
499 Classic, Siemens Healthineers, Erlangen, Germany) using a 32-channel receive head
500 coil (Nova Medical Head Coil, Wilmington, MA, USA). Functional data were acquired
501 with a T2*-weighted 2D gradient-echo EPI sequence (TR 2000 ms, TE 22 ms, 0.8 mm

502 isotropic voxels, number of slices 30, 90° flip angle, 128 X 128 mm² FOV, GRAPPA
503 acceleration factor 4, slice partial Fourier 5/8, coronal orientation, R>>L phase encoding
504 direction). Shimming was performed using the standard Siemens procedure. For the
505 first half of the sample, anatomical data were acquired using a MPRAGE sequence with
506 0.8 mm isotropic resolution (TR 2500 ms, TE 3.05 ms, TI 1050 ms, flip angle 5,
507 bandwidth 130 Hz/Px, 205 × 205 mm FOV, no GRAPPA applied, slice partial Fourier
508 6/8, base resolution 256, sagittal orientation, A>>P phase encoding direction, scan time
509 9 min 20 sec). For the second half of the sample, an additional T1-weighted image²
510 was acquired with the resolution of 0.7 mm isotropic voxels to provide a more precise
511 delineation of cerebro-spinal fluid and grey matter at the segmentation stage (TR 2500
512 ms, TE 2.55 ms, TI 1050 ms, flip angle 5, bandwidth 320 Hz/Px, 224 × 224 mm FOV,
513 GRAPPA factor 2, no partial Fourier, sagittal orientation, A>>P phase encoding
514 direction, time of acquisition 7 min 18 sec). Additional anatomical scans of
515 approximately 18 mins duration were acquired but not used here. During the functional
516 data acquisition, geometric distortions were corrected using EPI-PSF-based distortion
517 correction³. To correct for rigid-body motion, we applied prospective motion correction
518 during the acquisition of both structural and functional scans⁴. It is an optical in-bore
519 tracking system consisting of a single camera and marker. In order to establish a rigid
520 connection between the marker and head, a custom-made dental mouthpiece of the six
521 central teeth of the upper jaw has been crafted by the department of oral and
522 maxillofacial surgery of the university hospital of the Otto-von-Guericke university,
523 Magdeburg, Germany. The mouthpiece is equipped with an extension at which the
524 marker is attached. Therefore, line of sight between the marker and camera is never
525 lost.

526 1.5. Functional and anatomical data preprocessing

527 1.5.1. Bias field correction and segmentation of the anatomical image

528 The DICOM data were converted to NIfTI format using SPM 12 (Wellcome Trust Center
529 for Neuroimaging, University College London). The volumes were bias field-corrected
530 using a SPM-based customized script². To implement cortical depth-specific analysis,
531 we extracted grey matter segmentation for each subject. To do this, first we used the
532 SPM 12 segmentation algorithm and then the brainmask was generated by adding up
533 the white matter, grey matter and cerebro-spinal fluid masks. Then we applied the
534 FreeSurfer (version 6.0.0) recon algorithm to perform segmentation of white matter,
535 grey matter, generating their surfaces and a binary brain mask of the cortical ribbon (1 if
536 the voxel falls into the ribbon, 0 otherwise (steps 5-31 of recon-all algorithm)). We ran
537 the recon algorithm on the extracted brainmask from a T1-weighted image with a '-hires'
538 flag for the data with resolution higher than 1 mm^{2,3}. After running the recon algorithm,
539 the Freesurfer-generated grey and white matter segmentations were visually inspected

540 in each participant, the borders between CSF and grey matter as well as grey matter
541 and white matter were manually corrected within the region corresponding to the field of
542 view of functional scans. To improve segmentation quality, we performed the Freesurfer
543 segmentation algorithm not only on the T1-weighted image but also the T1-weighted
544 image divided by the PD-weighted contrast⁶. However, the T1-weighted image after the
545 division did not show essential advantages over using the data-driven bias field-
546 corrected T1-weighted image. Therefore, for the further cortical depth separation we
547 used the T1-weighted image without division.

548 1.5.2. Cortical depth and ROI definition

549 The grey matter segmentation acquired with Freesurfer was further utilized to obtain
550 cortical depth-specific compartments. Deep, middle and superficial compartments were
551 constructed using an equi-volumetric model^{7,8}. In order to analyze depth-specific
552 activity in early visual areas, we applied a probabilistic surface-based anatomical atlas⁸
553 to reconstruct the surfaces of areas V1, V2 and V3 separately for each region and
554 subject. This is an atlas of the visual field representation (eccentricity and polar angle),
555 and eccentricity values were used to select the foveal sub-part of the surface (0-3°). The
556 extracted surface ROIs (V1-V3) were then projected into the volume space and
557 intersected with the predefined cortical compartments. In this way, we obtained the V1,
558 V2 and V3 ROIs in the Freesurfer anatomical space at three predefined cortical depths.

559 1.5.3. Image alignment check

560 Functional volumes did not undergo any additional preprocessing. We did not
561 perform realignment due to utilization of prospective motion correction. However, we
562 ensured that the functional runs were well aligned with each other in each participant,
563 which is required for multivariate pattern analyses of high-resolution fMRI data, by
564 computing inter-run spatial cross-correlations of the signal intensities of the functional
565 volumes. For two participants an intensity-based image registration algorithm in
566 MATLAB was used to improve inter-run alignment until the inter-run correlations were at
567 least $r > .9$ on average. The resulting average spatial correlation of experimental runs
568 was (Mean \pm SD) 0.986 ± 0.01 , with the following motion parameters in the translation
569 and rotation directions (Mean \pm SD): x: -0.1 ± 0.3 , y: 0.2 ± 0.3 , z: -0.04 ± 0.3 , pitch: $-$
570 0.002 ± 0.003 , roll: -0.002 ± 0.005 , yaw: -0.000 ± 0.003 . Further, functional-anatomical
571 alignments were checked visually to ensure that the functional scans were well aligned
572 to the anatomical image at the location of the ROIs.

573 1.5.4. Registration

574 We linearly coregistered the extracted ROIs with predefined cortical depth
575 compartments to the EPI volumes within each subject using the Symmetric
576 Normalization (SyN) algorithm of ANTs¹⁰. Specifically, first, the T1-weighted anatomical

577 image was registered using linear interpolation to the EPI volume averaged over all the
578 functional runs. Next, we registered the ROIs with the predefined cortical depths to the
579 EPI volume applying the coordinate mapping (with the voxel size resampled to the
580 functional runs (0.8 isotropic)) obtained in the previous step (Figure 2C). In the resulting
581 ROIs the number of voxels per cortical depth (Mean \pm SD) was the following in V1:
582 $M_{\text{deep}}=1158\pm258$; $M_{\text{mid}}=1073\pm241$; $M_{\text{super}}=936\pm220$; in V2: $M_{\text{deep}}=1096\pm321$;
583 $M_{\text{mid}}=1049\pm260$; $M_{\text{super}}=901\pm319$; in V3: $M_{\text{deep}}=1123\pm364$; $M_{\text{mid}}=1019\pm256$;
584 $M_{\text{super}}=855\pm308$.

585 1.6. Multivariate pattern analysis

586 1.6.1. Data extraction

587 Multivariate pattern analysis (MVPA) was performed in each subject individually.
588 To prepare the EPI data for the MVPA, we first extracted activity patterns for each ROI
589 with the predefined cortical depths from the functional images in the main experiment
590 and orientation localizer run. Specifically, in each experimental run, we extracted voxel-
591 wise activation values for 3 oriented grating conditions (15°, 75° or 135°) and 12 trials
592 for each condition across 5 TRs (= 10 seconds), starting at trial onset. The EPI data
593 from the orientation localizer run was also aggregated for the 3 oriented grating
594 conditions (15°, 75° or 135°) and 15 trials per each condition across 5 TRs of trial
595 duration.

596 1.6.2. Classification

597 Multivariate pattern analysis (MVPA) was carried out using the linear support
598 vector machine ¹¹ (SVMs; libsvm: <http://www.csie.ntu.edu.tw/~cjlin/libsvm/>) with a fixed
599 cost parameter ($c=1$). We performed classification at each cortical depth and ROI
600 independently in the following way. We trained the SVM classifier on the fMRI data from
601 the orientation localizer run to discriminate between the 3 oriented gratings in each TR
602 separately using all the trials (15 data points per orientation per training set). Next, we
603 tested the SVM classifier using the EPI data from the main experiment (on each trial
604 separately). Each TR in orientation localizer task used for the classifier training
605 corresponded to the TR in the experimental trial used for the classifier testing. As a
606 result, we extracted predicted labels (15°, 75°, 135°) for every TR of all the trials in the
607 main experiment (chance level 33.3%). Then, we compared the labels predicted by the
608 SVM classifier with the oriented gratings actually presented, rotated or not used in each
609 trial (as illustrated in Figure 1C). The proportion of matches between the predicted
610 grating label and the role of that grating in the trial was accumulated over trials for each
611 of these three experimental conditions (presented, rotated and unused gratings) to
612 estimate their representational strength within each subject. Finally, the resulting

613 estimates in a form of 23 (subjects) x 3 (presented, rotated, not shown grating) x5 (TRs)
614 matrix calculated for each ROI and cortical depth was subjected to statistical testing.

615 Note that in our paradigm the three orientations on each trial are not
616 independent. The more information about one of the orientations is found (e.g., the
617 perceived orientation), the less information is found about the other orientations (e.g.,
618 the rotated orientation). We therefore cannot compare classifier choices to “chance”
619 level (i.e., 33%). Instead, we compare classifier choices for these orientations to the
620 third, unused orientation. This procedure allowed us to estimate information about the
621 perceived and rotated orientations independently from each other. For instance, if the
622 representation of the perceived orientation is so strong that the classifier very often
623 picks the perceived orientation, it may be that the classifier picks the rotated orientation
624 in fewer than 33% of trials. However, this does not mean that there is no information
625 about the rotated orientation: If there are still more classifier choices for the rotated
626 orientation than the unused orientation, the rotated orientation is represented in the
627 signal.

628 For the in-depth assessment of mental rotation contents, a critical time interval
629 was chosen based on the previous studies⁴⁻⁵ where mentally rotated representations
630 could be decoded in the period 8-12 seconds after the rotation cue. In our study, we
631 included time interval 8-10 s after the rotation cue since the measurement at 12 s was
632 likely to carry the representation of a probe grating (shown at 8 s), while the
633 measurement at 10 s is too close to the presentation of the probe grating to be
634 contaminated by it.

635 1.6.3. Statistical testing

636 We used repeated-measures analyses of variance (ANOVA) to test the main
637 effect of Signal type (presented vs mentally rotated grating) in the trial and to test the
638 interaction of Signal type and Cortical depths (deep and superficial vs. middle) (custom
639 function `rmanova2` derived by A. Schurger (2005) from Keppel & Wickens, “Design and
640 Analysis”, ch.18: [https://de.mathworks.com/matlabcentral/fileexchange/6874-two-way-](https://de.mathworks.com/matlabcentral/fileexchange/6874-two-way-repeated-measures-anova)
641 `repeated-measures-anova`). In cases where the assumption of sphericity was violated
642 the p-values were corrected using a Huynh-Feldt correction (provided as an output of
643 the same function). Significant interactions were followed up with paired-samples one-
644 sided t-tests (`ttest` function in MATLAB) to analyze the effects in the assumed directions
645 based on neuroanatomy and animal findings. To control for multiple comparisons
646 across t-tests, we used FDR-corrections that assume independent or positively
647 correlated tests¹²: these corrections allow for maintaining a low false positive rate while
648 providing reasonable power to find truly significant results.

649 1.7. Data availability

650 The MRI and behavioral data that were used in this study are available:
651 https://osf.io/3x9fk/?view_only=dd7d8e9462694501a60a4dd308fd9354.

652 1.8. Code availability

653 MATLAB source code for LIBSVM toolbox is available online (libsvm:
654 <http://www.csie.ntu.edu.tw/~cjlin/libsvm/>). The code for data sorting and utilizing this
655 toolbox in the present study will be provided upon acceptance.

656 1.9. Methods references

- 657 1. Brainard, D. H. (1997) The Psychophysics Toolbox, *Spatial Vision* 10:433-436.
- 658 2. Luesebrink, F., Sciarra, A., Mattern, H. et al. T1-weighted in vivo human whole brain
659 MRI dataset with an ultrahigh isotropic resolution of 250 μm . *Sci Data* 4, 170032
660 (2017). <https://doi.org/10.1038/sdata.2017.32>
- 661 3. Zaretskaya, N., Fischl, B., Reuter, M., Renvall, V., Polimeni, J.R., 2017. Advantages
662 of cortical surface reconstruction using submillimeter 7 T MEMPRAGE. *Neuroimage*.
663 doi:10.1016/j.neuroimage.2017.09.060
- 664 4. In, M. H., & Speck, O. (2012). Highly accelerated PSF-mapping for EPI distortion
665 correction with improved fidelity. *Magnetic Resonance Materials in Physics, Biology*
666 *and Medicine*, 25(3), 183-192.
- 667 5. Maclaren, J., Armstrong, B. S., Barrows, R. T., Danishad, K. A., Ernst, T., Foster, C.
668 L., Gumus, K., Herbst, M., Kadashevich, I. Y., Kusik, T. P., Li, Q., Lovell-Smith, C.,
669 Prieto, T., Schulze, P., Speck, O., Stucht, D., & Zaitsev, M. (2012). Measurement
670 and correction of microscopic head motion during magnetic resonance imaging of
671 the brain. *PloS one*, 7(11), e48088. <https://doi.org/10.1371/journal.pone.0048088>
- 672 6. Van de Moortele, P. F., Auerbach, E. J., Olman, C., Yacoub, E., Uğurbil, K., &
673 Moeller, S. (2009). T1 weighted brain images at 7 Tesla unbiased for Proton
674 Density, T2* contrast and RF coil receive B1 sensitivity with simultaneous vessel
675 visualization. *NeuroImage*, 46(2), 432–446.
676 <https://doi.org/10.1016/j.neuroimage.2009.02.009>
- 677 7. Waehnert, M. D., Dinse, J., Weiss, M., Streicher, M. N., Waehnert, P., Geyer, S., ...
678 Bazin, P. L. (2014). Anatomically motivated modeling of cortical laminae.
679 *NeuroImage*, 93, 210–220. <https://doi.org/10.1016/j.neuroimage.2013.03.078>
- 680 8. Huntenburg, J. M., Steele, C. J., & Bazin, P. L. (2018). Nighres: processing tools for
681 high-resolution neuroimaging. *GigaScience*, 7(7), giy082.
- 682 9. Benson NC, Butt OH, Brainard DH, Aguirre GK (2014) Correction of distortion in
683 flattened representations of the cortical surface allows prediction of V1-V3 functional
684 organization from anatomy. *PLoS Comput. Biol.*

- 685 10. Avants, B. B., Epstein, C. L., Grossman, M., & Gee, J. C. (2008). Symmetric
686 diffeomorphic image registration with cross-correlation: evaluating automated
687 labeling of elderly and neurodegenerative brain. *Medical image analysis*, 12(1), 26–
688 41. <https://doi.org/10.1016/j.media.2007.06.004>
- 689 11. Müller, K.R., Mika, S., Räscht, G., Tsuda, K. & Schölkopf, B. (2001) An introduction
690 to kernel-based learning algorithms. *IEEE Trans. Neural Netw.* 12, 181–201
- 691 12. Benjamini, Y., & Yekutieli, D. (2005). False discovery rate-adjusted multiple
692 confidence intervals for selected parameters. *Journal of the American Statistical*
693 *Association*, 100(469), 71-81.

694

695 Acknowledgments: PI is supported by the Berlin School of Mind and Brain PhD
696 scholarship. DK and RMC are supported by Deutsche Forschungsgemeinschaft (DFG)
697 grants (KA4683/2-1, CI241/1-1, CI241/3-1). RMC is supported by a European Research
698 Council Starting Grant (ERC-2018-StG). NW was supported by the European Research
699 Council under the European Union's Seventh Framework Programme (FP7/2007-2013)
700 / ERC grant agreement n° 616905; the European Union's Horizon 2020 research and
701 innovation programme under the grant agreement No 681094; the BMBF (01EW1711A
702 & B) in the framework of ERA-NET NEURON. We thank the staff of the Department of
703 Oral and Maxillofacial Surgery, University Hospital Magdeburg A.ö.R., Christian Zahl,
704 Indra Griesau and Christine Rohloff for creating individually custom made removable
705 dental braces. Computing resources were provided by the high-performance computing
706 facilities at ZEDAT, Freie Universität Berlin.

707

708 Author contributions: P.I., D.K. and R.M.C. designed the study, R.M.C., E.D., O.S., N.W.
709 supervised the study, P.I., R.Y., A.S., H.M. and F.L. acquired data. P.I., D.K., D.H., and
710 F.L. analyzed the data. P.I., D.K., R.M.C. wrote the original draft of the manuscript,
711 R.Y., A.S., H.M., F.L., E.D., O.S., N.W. reviewed and edited the manuscript.

712

713 Materials and Correspondence: Correspondence and requests for materials should be
714 addressed to iamshchinina@gmail.com.

715

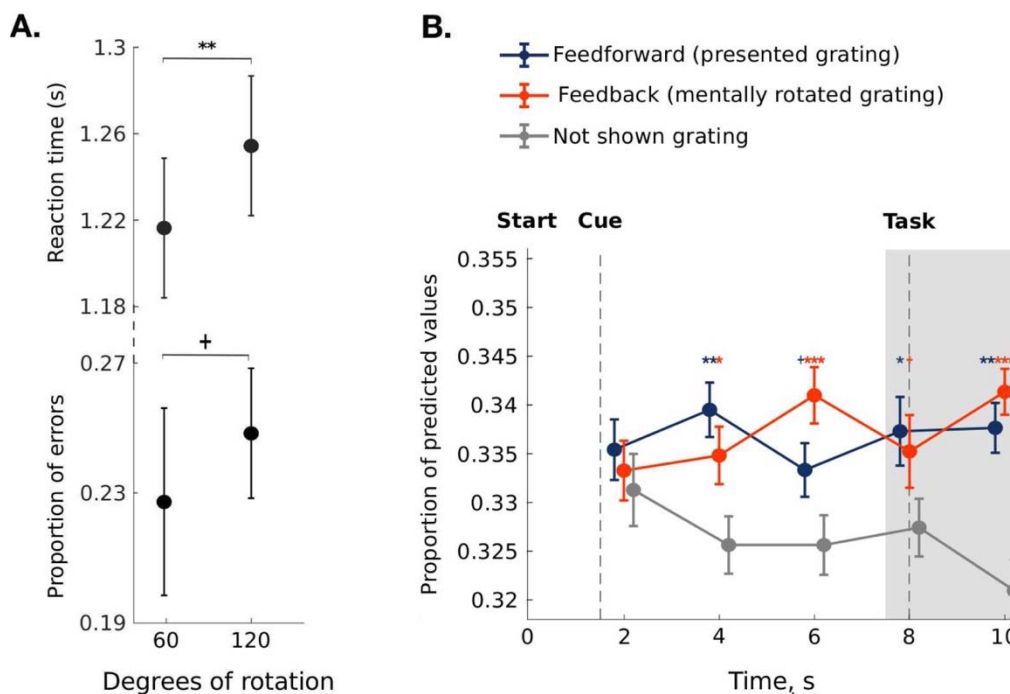
716 Competing interests: The authors declare no competing interests.

717

718 Additional Information: Correspondence and requests for materials should be
719 addressed to iamshchinina@gmail.com. Reprints and permissions information is
720 available at www.nature.com/reprints

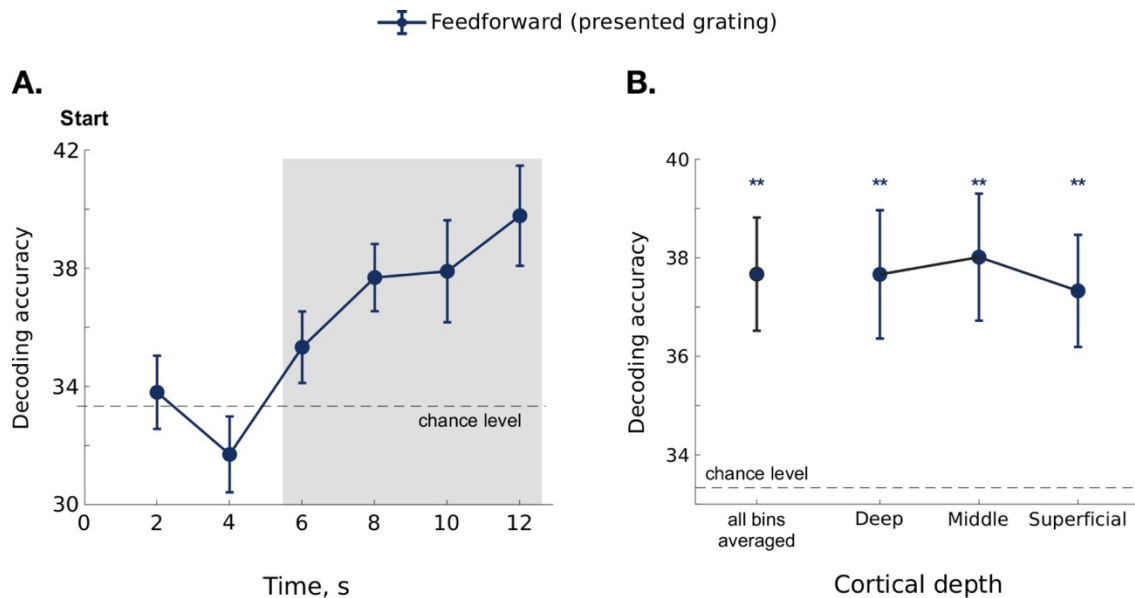
721

722 **Supplementary Data**



723

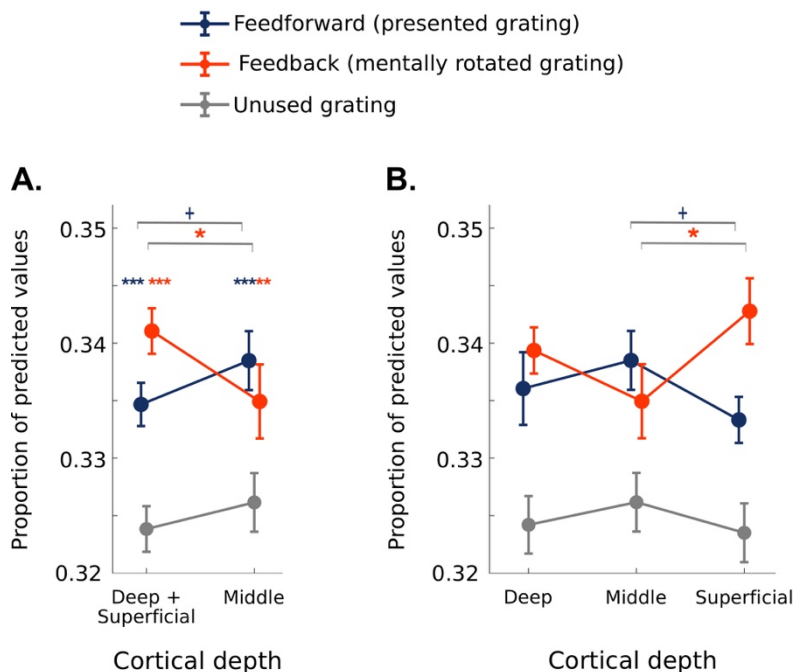
724 **Supplementary Figure 1.** Behavioral results and classifier decisions in V1. **A.** Reaction time was shown
725 to be slower and error rate to be higher when responding to the probe after 120° mental rotation
726 compared to 60°¹. +: $p < 0.07$, **: $p < 0.01$. **B.** To establish the concurrent representation of perceived and
727 mentally rotated contents in V1 we averaged classifier predictions across the cortical depths. This yielded
728 three time courses, reflecting how often classifiers predicted the orientation of the presented, the rotated
729 and the unused gratings. To estimate the presence of perceptual representations, we ran a 2x2 repeated
730 measures ANOVA with factors Signal Type (perceived vs. unused grating) and Time Points (4,6,8, and 10
731 seconds after onset). In this time interval, perceptual representations were evident from a significant main
732 effect of Signal Type (Figure 2B, $F_{1,66}=15.3$, $p=0.0007$). To estimate the presence of feedback signals, we
733 ran a similar ANOVA, now comparing the proportion of predictions for the rotated grating and the unused
734 gratings. We also obtained a significant main effect of Signal Type for the mentally rotated contents
735 (Figure 2B, $F_{1,66}=21.55$, $p=0.0001$). We also provide the results of the t-tests for every time point
736 (uncorrected for multiple comparisons). Both perception and rotation signals were similar across the time
737 points examined (interaction with time, both $F < 1.27$). When comparing representations of perceived and
738 rotated contents, no significant differences were found ($F=0.16$), also when considering individual time
739 points (all $t < 1$). These results establish the presence of feedforward and feedback signals in V1. All error
740 bars denote standard error of the mean over subjects. +: $p < 0.09$, *: $p < 0.05$, **: $p < 0.01$, ***: $p < 0.001$.
741



742

743 **Supplementary Figure 2. Decoding orientation information from the perceptual localizer task in**
744 **V1. A.** The time series of perception signal averaged across all grey matter bins. In order to establish the
745 representation of perception signal in the localizer task, we trained a three-class classifier to differentiate
746 between the three grating orientations using all the trials in the run leaving one trial out. Start denotes the
747 start of the 12 seconds trial in the perceptual localizer task. The shaded area highlights the time points
748 selected for the further depth-specific analysis. **B.** Classifier decisions over the measurements at 6, 8, 10
749 and 12 seconds after the trial onset across the cortical depth bins reveal robust neural information about
750 the feedforward perceived orientation ($F_{1,66} = 909.68$, $p=2.2e-19$). We also found significant
751 representation of orientation information in each depth bin separately (for deep: $t_{22}=3.33$, $p=0.0015$,
752 middle: $t_{22}=3.62$, $p=0.0015$, superficial: $t_{22}=3.51$, $p=0.0015$); however, no difference between the
753 different bins was found. Horizontal line represents a chance level (33,33%) against which the decoding
754 accuracy estimates were tested. All error bars denote standard error of the mean over subjects. *: $p<0.05$,
755 **: $p < 0.01$, ***: $p < 0.001$.

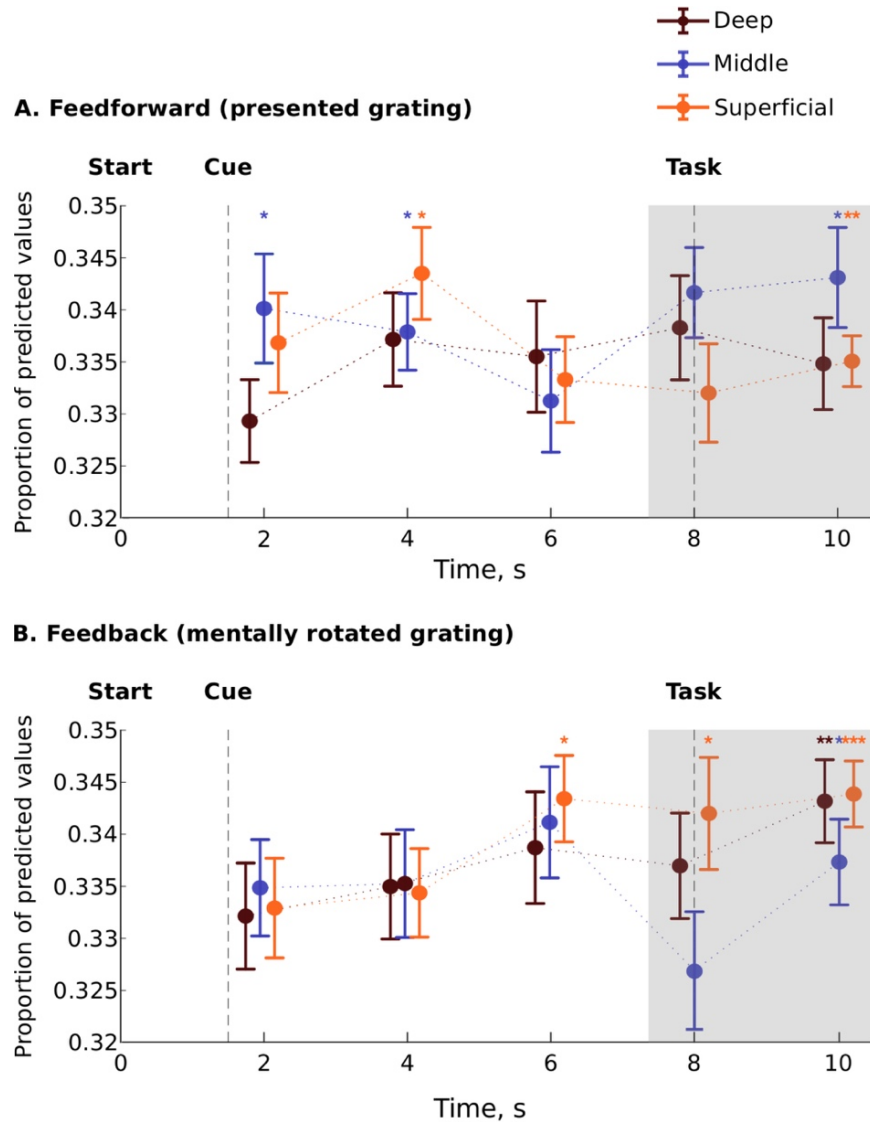
756



757

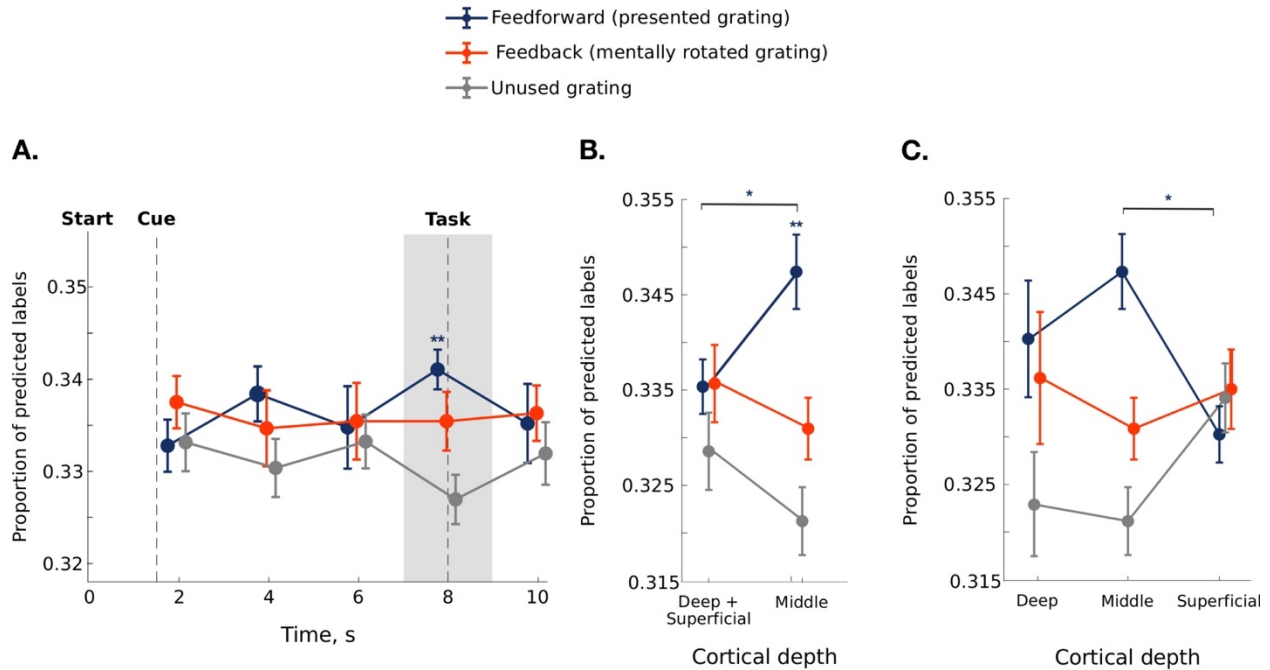
758 **Supplementary Figure 3. Classifier decisions in V1 at an extended time interval (6, 8 and 10 sec.)**

759 **after trial onset.** Since in our experiment we find a representation of mental rotation already at 6 seconds
760 after rotation cue, we also provide the in-depth analysis for the time interval comprising measurements at
761 6, 8 and 10 seconds. **A.** At the time interval spanning 6,8 and 10 seconds, we found a strong
762 representation of mental rotation contents in the outer cortical bins ($t=5.4$, $p=1*10^{-5}$, Cohen's $d=0.99$)
763 and a trend in the middle bin ($t=1.7$, $p=0.05$, Cohen's $d=0.35$). The feedforward signal was significantly
764 above unused grating in all the cortical bins (at the middle depth: $t=3.1$, $p=0.008$, Cohen's $d=0.65$; at the
765 outer depths: $t=3.6$, $p=0.0008$, Cohen's $d=0.75$), in accordance with the results at the initially chosen time
766 interval in Fig.2A. The 2x2 Depth-by-Signal interaction was at the level of trend ($F=3.4$, $p=0.078$).
767 Specifically, the outer cortical bins carried mental rotation representation compared to the middle depth
768 ($t=1.8$, $p=0.04$, Cohen's $d=0.38$) and a trend towards more strongly represented perception signal than
769 mentally rotated gratings was found at the middle cortical depth ($t=1.6$, $p=0.06$, Cohen's $d=0.32$).
770 Additionally, a direct comparison of the two signal types in the outer cortical bins revealed more strongly
771 represented mentally rotated contents compared to the perceived ones ($t=1.8$, $p=0.04$, Cohen's $d=0.38$)
772 indicating an exclusive role of outer cortical depths in carrying feedback signal. **B.** Separate analysis
773 across the three cortical depths revealed a significant 2x2 Depth-by-Signal interaction between the middle
774 and superficial cortical bins ($F=7.1$, $p=0.01$), with superficial depth carrying stronger mental rotation
775 representation in comparison to middle depth ($t=2.3271$, $p=0.04$, Cohen's $d=0.5$) and middle depth
776 predominantly representing feedforward signal ($t=2$, $p=0.07$, Cohen's $d=0.4$). Additionally, in the
777 superficial bin we found a stronger representation of mentally rotated contents than perceived ones
778 ($t=2.24$, $p=0.02$, Cohen's $d=0.47$) confirming the predominant role of superficial cortical bin in supporting
779 mental rotation feedback. The 2x2 Depth-by-Signal interaction between the middle and deep cortical bins
780 as well as the 3x2 Depth-by-Signal interaction did not reach significance. Overall, including three time
781 points in the in-depth analysis gives qualitatively similar Signal-by-Depth dissociation as in the main
782 analysis (Fig.2) where mentally rotated contents are more strongly represented in the outer bins, mainly
783 at the superficial depth, and perception contents are present across all the three depths. All error bars
784 denote standard error of the mean over subjects. +: $p<0.09$, *: $p<0.05$, **: $p<0.01$, ***: $p<0.001$.



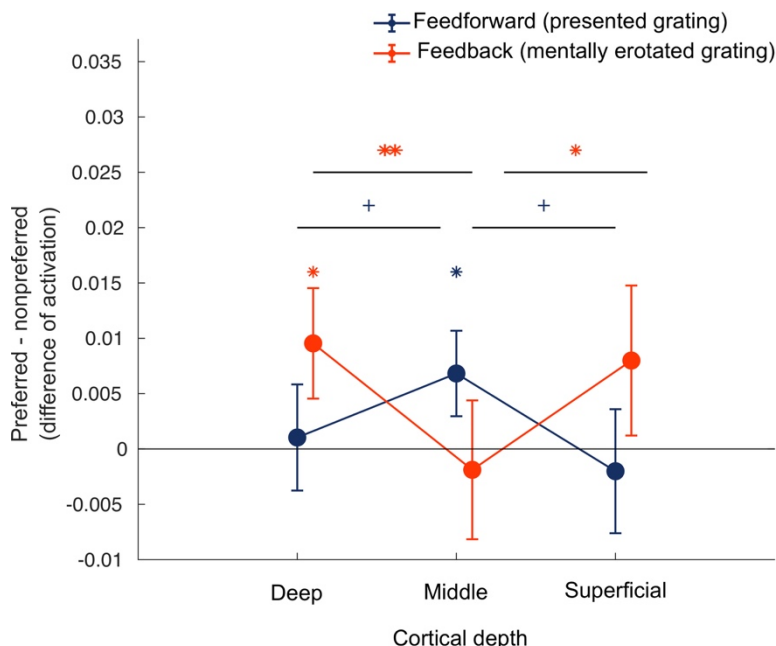
785

786 **Supplementary Figure 4. Depth-specific time series of classifier decisions in area V1 plotted**
787 **separately for feedforward (A) and feedback signals (B).** As in the main analysis, classifier decisions
788 for the perceived and rotated orientation were tested against decisions for the unused orientation (not
789 shown here to avoid clutter). Grey area highlights the time interval chosen for the main analysis. All error
790 bars denote standard error of the mean over subjects. *: $p < 0.05$, **: $p < 0.01$, ***: $p < 0.001$ (uncorrected
791 for multiple comparisons).



792

793 **Supplementary Figure 5. Classifier decisions for mental rotation and perception information in**
794 **area V2. A.** Analysis of time courses of classifier estimates averaged across cortical depths, revealed a
795 significant decoding of visual perception contents in area V2 measured at 8 seconds after the trial onset
796 ($t_{22}=3.83$, $p=0.002$). We found no significant decoding of mentally rotated contents in area V2 and V3.
797 The shaded area denotes the time point selected for the further depth-specific analysis. **B.** Classifier
798 decisions over the time interval from 6 to 8 seconds after the trial onset for the presented, mentally
799 rotated and unused gratings in the middle and outer depths (averaged superficial and deep). The analysis
800 revealed significant representation of the perceived contents at the middle cortical depth ($t_{22}=3.9$,
801 $p=0.0012$) compared to the unused grating. Furthermore, a stronger perception signal was found in the
802 middle cortical bin compared to the outer bins ($t_{22}=2.24$, $p=0.035$). **C.** Analysis across all the three cortical
803 depths separately revealed a more strongly represented feedforward signal at the middle depth compared
804 to the superficial one ($p<0.05$). All error bars denote standard error of the mean over subjects. *: $p<0.05$,
805 **: $p < 0.01$.



806
807

808 **Supplementary Figure 6. Signal-by-Depth interaction analyzed with a univariate approach.** We
809 sorted the voxels in each cortical depth by their preference towards each of the three grating
810 based on the voxel activations in the orientation localizer task. We then picked the 300 most orientation-
811 preferring voxels for each of the three orientations. To quantify the rotation signal, we then calculated the
812 difference between the activation for rotated grating and two other gratings (non-preferred) within the
813 voxels which preferred the rotated grating condition. To quantify the perception signal, we calculated the
814 difference between the activation for perceived grating and two other gratings within the voxels which
815 preferred the perceived grating condition. Prior to the analysis, the voxel responses both in the orientation
816 localizer task and in the main experiment were high-pass filtered using spm12. We found a signal X depth
817 interaction (3X2 interaction: $F(2,44)=3.34$, $p=0.04$; 2X2 interaction: $F(1,22)=6.5$, $p=0.02$), showing
818 stronger rotation information in the superficial and deep cortical bins and stronger perception information
819 at the middle depth. In detail, perception signal was significantly above 0 at the middle cortical depth
820 ($t(22)=1.8$, $p=0.05$, Cohen's $d=0.37$) and trended to be stronger than in the outer bins (middle vs. deep
821 bins: $t(22)=1.6$, $p=0.06$ Cohen's $d=0.33$; middle vs. superficial bins: $t(22)=1.6$, $p=0.06$, Cohen's $d=0.34$).
822 The rotation signal was significantly above 0 in the deep bin ($t(22)=1.9$, $p=0.03$, Cohen's $d=0.4$) and
823 stronger in the outer bins than the middle bin (middle vs. deep bin: $t(22)=2.6$, $p=0.007$, Cohen's $d=0.55$;
824 middle vs. superficial bin: $t(22)=1.8$, $p=0.04$, Cohen's $d=0.37$).

825

826